PAPER

Check for updates

Boron nitride-based magnetic nanocomposite for magnetic solid-phase extraction coupled with HPLC-UV for simultaneous determination of three tetracyclines in pork, egg, and milk

Junmei Li,† Weiran Wang,† Yupeng Sun, Yan Fu, Haoqi Zhang, Bingrong Wang, Chunying Wang* and Xue Xiong [ID] *

Tetracycline antibiotic residue in food is of vital significance for public health. Hexagonal boron nitride (h-BN)-based materials are excellent absorbents for antibiotics, and modification of the h-BN surface would improve its adsorption ability. In this study, a Fe_3O_4-modified h-BN nanocomposite (Fe_3O_4@h-BN) was fabricated by a simple one-step coprecipitation method. The nanocomposite was characterized by scanning electron microscopy (SEM), X-ray diffraction (XRD), Fourier transform infrared (FT-IR) spectroscopy, and vibrating sample magnetometer (VSM). Fe_3O_4@h-BN was used as a magnetically recyclable adsorbent for magnetic solid phase extraction (MSPE) of tetracycline (TC), oxytetracycline (OTC), and chlortetracycline (CTC), and the adsorption performance was investigated under different influencing factors, including contact time, adsorbent dosage, pH conditions, and ionic strength. The nanocomposite Fe_3O_4@h-BN was used for the analysis of three tetracyclines (TCs) in pork, egg, and milk samples using MSPE coupled with high-performance liquid chromatography equipped with a UV detector (HPLC-UV). Under the optimized experimental conditions, the recoveries measured for pork, egg, and milk samples ranged from 84.2% to 96.6%, 92.8% to 108.2%, and 84.1% to 102.6%, respectively, with relative standard deviations (RSDs) of 0.3–9.4%, 0.8–9.7%, and 1.3–7.1%, respectively. This work presents a simple and effective method for antibiotic analysis in food samples.

1. Introduction

In recent years, antibiotics have been extensively used to improve the health of animals and humans, and as growth promoters for livestock, bees, aquatic products, and other aquaculture industries.[1] Tetracycline antibiotics (TCs) are an entire group of antibiotics and include tetracycline (TC), oxytetracycline (OTC), and chlortetracycline (CTC), which are some of the most widely used for therapeutic purposes to take advantage of their broad spectrum of activity, high quality, ease of use, and low cost.[2,3] TCs control animal diseases and are a major antibiotic additive in agricultural feed. However, residues of TCs may accumulate in food products such as honey,[4] meat, milk,[5] and eggs.[6,7]

Excessive intake of TCs poses human health risks such as liver and kidney damage, negative impacts upon the teeth,[8] and chronic conditions such as obesity, diabetes, and inflammatory bowel disease.[5] Moreover, TCs may lead to significant environmental risks due to their accumulation in the food chain, and

may cause adverse effects on human health such as bacterial resistance.[9] As a result of growing concerns that have been raised about public health issues due to the presence of TCs in foods, it is urgent that an effective, reliable, and economical technique be established for the determination of TCs in food samples.

TC antibiotics exist in foods at trace levels, and because the matrix is always complex, proper sample pretreatment techniques are essential prior to instrumental analysis to obtain satisfactory instrument performance and results.[7,10,11] Magnetic solid phase extraction (MSPE) is a new solid phase extraction (SPE) technique that has become a prospective sample pretreatment method. In this mode, magnetic nanoparticle (MNP) adsorbents can be separated from sample solutions under an external magnetic field after dispersion in sample solutions, and the analytes are then desorbed from the MNPs by an appropriate eluting solvent.[12,13] Unlike traditional column SPE and non-magnetic adsorbents, the adsorbent separation is convenient and easy, and adsorbent packing, centrifugation, and filtration sample pretreatment processes are not necessary.[14,15] However, magnetic adsorbents are the key factor that affect the extraction efficiency and selectivity of the method. In addition, the stability of magnetic adsorbents can affect the

School of Pharmacy, Hebei Medical University, Shijiazhuang 050017, People's Republic of China. E-mail: wangcy730301@163.com; xiongxue@hebmu.edu.cn

† These authors contributed equally to this work.

recycling performance, which is economical and eco-friendly. TCs can be adsorbed by a magnetic provider such as bare Fe_3O_4 through chelate interaction.[16] By coupling with a promising base material to fabricate a significant magnetic composite adsorbent, this provides the advantages of the magnetic and the selected base material, such as excellent adsorption characteristics and easy separation by external magnetic field.[17–19]

Hexagonal boron nitride (h-BN) is a chemical compound constructed from equal numbers of boron (B) and nitrogen (N) atoms, and this typical two-dimensional material with a graphene-like structure is referred to as 'white graphene'.[20,21] With its high thermal and chemical stability, advantageous optical and mechanical properties, and high oxidation resistance, h-BN can serve as a potential adsorbent.[22,23] The alternating B and N atoms are covalently bonded to each other in a honeycomb arrangement, and compared to graphene, the adsorption ability of h-BN is unique.[24] The h-BN material can build strong interactions with aromatic analytes through $\pi-\pi$ interaction,[25] and stronger dipole–dipole interactions through the polar h-BN surface.[24]

The h-BN surfaces modified with metal ions can enhance adsorption.[26–28] In the field of magnetic solid-phase extraction (MSPE), h-BN-based materials have been explored as adsorbents in several studies.[21,29,30] However, there have been few reports describing the application of Fe_3O_4-functionalized h-BN composites (Fe_3O_4@h-BN) for the detection of TCs. The flexible 2D structure of h-BN nanosheets not only accommodates volume changes of Fe_3O_4 nanoparticles during redox processes, but it also effectively prevents their aggregation.[31,32] Given these advantages, developing a simple and efficient method for the synthesis of Fe_3O_4@h-BN magnetic nanomaterials as MSPE adsorbents could significantly enhance TC analysis in real-world samples, offering substantial research and practical value.

In this work, a one-step coprecipitation method was used to synthesize magnetically separable Fe_3O_4@h-BN composites. Unlike conventional hydrothermal approaches that typically require harsh conditions (150–250 °C, 12–24 h), this strategy enables efficient h-BN modification under low heating (80 °C) through direct precursor mixing, with a significantly reduced reaction time of 6 h.[30,33] The physical and chemical properties were characterized by scanning electron microscopy (SEM), X-ray powder diffraction (XRD), and Fourier transform infrared (FT-IR) spectroscopy. To achieve the highest extraction efficiency, a series of main parameters such as pH and ionic strength were optimized. Finally, a Fe_3O_4@h-BN-based MSPE method combined with HPLC-UV was developed for detection of TCs in pork, egg, and milk, and this technique is selective, rapid, convenient, cost-effective, and environmentally benign.

2. Experimental

2.1. Materials and instruments

HPLC-grade methanol and acetonitrile were procured from Scharlau (Barcelona, Spain). Hexagonal boron nitride (h-BN, 99.9%), oxytetracycline hydrochloride (TC, 99.9%),

oxytetracycline dihydrochloride (OTC, 99.9%), and chlortetracycline hydrochloride (CTC, 99.9%) were purchased from Shanghai Macklin Biochemical Co., Ltd. Ferric chloride ($FeCl_3$) and ferrous sulfate ($FeSO_4 \cdot 7H_2O$) were purchased from Tianjin Kemao Chemical Reagent Co., Ltd. All other reagents were purchased from Sinopharm Chemical Reagent Co., Ltd. All chemicals used were of analytical or HPLC grade. Ultrapure water was prepared using the Milli-Q50 water purification system (Millipore, Bedford, MA, USA) and used throughout the experiments. Samples for HPLC analysis were filtered through a 0.45 μm membrane filter. Milk, eggs, and pork samples were purchased from a supermarket (Hebei, China).

2.2. Synthesis of Fe_3O_4@h-BN

The nanoparticles were synthesized by a co-precipitation method. A mixture of $FeCl_3$ (0.383 g) and $FeSO_4 \cdot 7H_2O$ (0.328 g) was added to $NH_3 \cdot H_2O$ solution (50 mL, pH 11.0). The solution was heated to 80 °C and then stirred to react for 6 h. The magnetic precipitate was washed thrice with water, collected with a magnet, and dried under vacuum at 60 °C for 12 h. Subsequently, Fe_3O_4@h-BN was synthesized by a similar method. $FeCl_3$ (0.383 g), $FeSO_4 \cdot 7H_2O$ (0.328 g), and h-BN (0.5 g) were added to a solution of $NH_3 \cdot H_2O$ (50 mL, pH 11.0). The solution was heated to 80 °C, and then stirred to react for 6 h. The magnetic precipitate was washed thrice with water, and Fe_3O_4@h-BN was collected with a magnet, and then dried under vacuum at 60 °C for 12 h.

2.3. Apparatus

The Fourier transform infrared (FT-IR) spectra of the prepared particles within the wavenumber range of 400–4000 cm^{-1} were acquired using a Shimadzu IRAffinity-1S spectrometer (Japan) with KBr pellet preparation. Surface morphologies were characterized *via* field-emission scanning electron microscopy (FE-SEM, GeminiSEM 500, Zeiss, Germany). The magnetic properties were evaluated at room temperature using a vibrating sample magnetometer (VSM, MPMS3, Quantum Design, USA). Crystalline phase analysis was performed by X-ray diffraction (XRD, Rigaku SmartLab, Japan). The Brunauer–Emmett–Teller (BET) surface area analysis was performed using a Micromeritics ASAP 2460 analyzer (Micromeritics, USA). X-ray photoelectron spectroscopy (XPS) measurements were carried out on a Thermo Scientific K-Alpha spectrometer (Thermo Fisher Scientific, USA).

2.4. MSPE procedure and HPLC analysis

Adsorption isotherm tests were conducted using a series of concentrations (10–700 μg mL^{-1}) of the three antibiotics (TC, OTC, and CTC). Adsorption kinetics research was conducted at a concentration of 400 μg mL^{-1}. To prepare the 0.1 mol per L Na_2EDTA–McIlvaine buffer solution, 60.50 g of disodium ethylenediaminetetraacetate (Na_2EDTA) was dissolved in 1625 mL of McIlvaine buffer solution. McIlvaine buffer solution was prepared by mixing 1000 mL of 0.1 mol per L citric acid with 625 mL of 0.2 mol per L Na_2HPO_4, followed by pH adjustment to

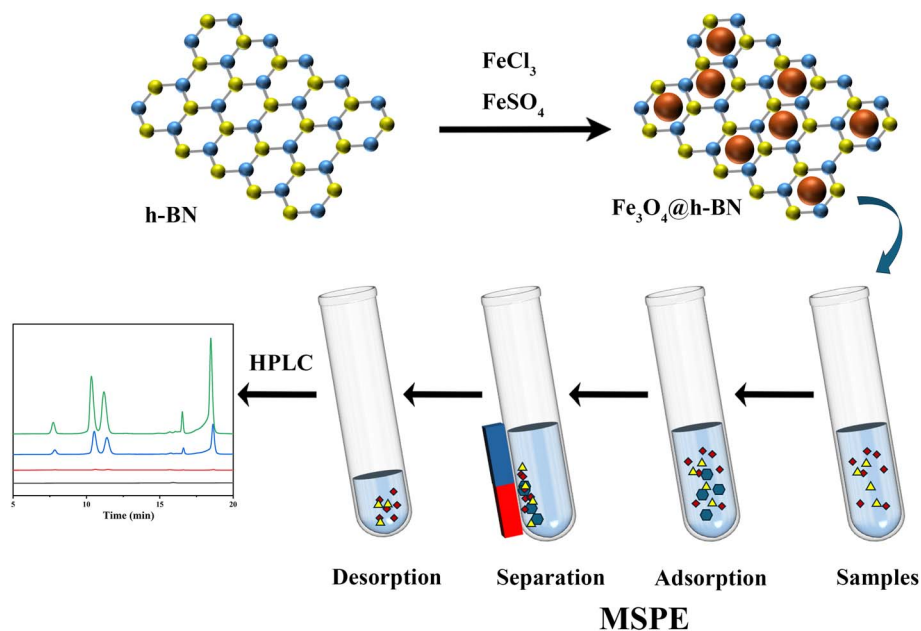**Fig. 1** Synthesis of Fe$_3$O$_4$@h-BN and its application as an MSPE adsorbent for determination of TCs by HPLC.

4.0 using 1.0 mol per L HCl or NaOH. The MSPE process is shown in Fig. 1.

The adsorption experiments were carried out in 10 mL polypropylene tubes. The samples for adsorption studies were prepared by adding 50 mg of adsorbent to 5 mL of analyte solution. All samples were maintained inside a VORTEX MS3 Multifunctional Vortex Mixer (Lepte Scientific, China) at 25 °C and 500 rpm. At the end of equilibrium, the sample solutions were exposed to a magnetic field for analysis. For eluate analysis, the absorbents separated with magnets were eluted with 500 μL of acetonitrile–methanol–0.5% formic acid–EDTA buffer solution–water (4 : 1 : 2 : 0.5 : 2.5) for 2 min under ultrasound. The eluent was filtered using 0.45 μm filter membrane and subsequently analyzed by HPLC-UV.

HPLC analysis was performed using an ArcHPLC-2998 HPLC-UV instrument (Waters, USA), which was equipped with a reversed-phase C18 HPLC column (5 μm, 250 mm × 4.6 mm, Agela, USA). The separation conditions were as follows: injection capacity at 20 μL, column temperature at 30 °C, flow rate of 1 mL min^{-1}, the mobile phase consisted of pure methanol (mobile phase A) and water containing 0.01 mol per L oxalic acid solution (mobile phase B), and the gradient elution was performed with the following program: 0–12 min, 75% B; 12–21 min, 60% B; 21–25 min, 75% B.

2.5. Adsorption studies

The adsorption capacity at equilibrium was determined by the following equation:

$$Q = (c_0 - c_e)V/m$$

where Q (mg g^{-1}) represents the amount of adsorption at equilibrium, c_0 and c_e (mg L^{-1}) denote the initial and equilibrium concentrations of the adsorbates, respectively, V (L)

denotes the volume of the solution, and m (g) denotes the mass of the adsorbent. All the adsorption experiments reported in this study were performed in triplicate.

2.5.1. Adsorption isotherm study. Adsorption isotherm studies were conducted by adding 50 mg of Fe$_3$O$_4$@h-BN to 5 mL of the three TC antibiotic solutions with different concentrations (10–700 μg mL^{-1}). The adsorption isotherm data were analyzed using Langmuir and Freundlich isotherm models that are expressed by the following equations:

Langmuir adsorption isotherm:

$$Q = Q_m K_L c/(1 + K_L c)$$

Freundlich adsorption isotherm:

$$Q = K_F c^{1/n}$$

where Q (mg g^{-1}) represents the amount of adsorption at equilibrium, K_L (mL mg^{-1}) denotes the Langmuir adsorption equilibrium constant related to the free energy of adsorption, c denotes the equilibrium concentration of the TCs in solution, Q_m (mg g^{-1}) denotes the maximum adsorption capacity of Fe$_3$O$_4$@h-BN, and K_F and n denote constants that measure the adsorption capacity and sorption energy, respectively. The Langmuir model assumes that the analytes are adsorbed on the adsorbent in the form of a monolayer, while the Freundlich model assumes multilayer adsorption.

2.5.2. Kinetics of adsorption. The kinetic studies were conducted by adding 50 mg of Fe$_3$O$_4$@h-BN adsorbent to 5 mL of the three TC antibiotic solutions at a concentration of 400 μg mL^{-1}. The stock solutions were subjected to oscillation frequency at 500 rpm for different amounts of time (0.5–15 min). Furthermore, the experimental data were fitted into

pseudo-first order and pseudo-second order kinetic models to determine the adsorption kinetic parameters by the following equations:

Pseudo-first order:

$$Q = Q_e(1 - e^{-K_1 t})$$

Pseudo-second order:

$$Q = t/(1/(K_2 Q_e^2) + t/Q_e)$$

where K_1 (min^{-1}) denotes the pseudo-first order rate constant, and K_2 denotes the pseudo-second order kinetic rate constant.

2.6. Preparation of real samples

To prepare real samples, 5 g of homogenized milk, egg, and pork were each placed in a 50 mL centrifuge tube. The samples were extracted by adding 10 mL of acetonitrile and 10 mL of Na_2EDTA–McIlvaine buffer to the tube and vortexing for 10 min under ultrasonic extraction. The samples were then centrifuged at a low temperature of 4 °C and 9000 rpm for 5 min, and the upper layer extract was collected in a 100 mL polypropylene tube. The extraction was repeated twice, and the two extracts were then combined. All extracts were filtered through a 0.45 μm filter for follow-up MSPE procedures.

3. Results and discussion

3.1. Characterization

The external morphologies of h-BN and Fe_3O_4@h-BN were analyzed and compared by SEM. Fig. 2A and B show that h-BN assumes a regular layered structure. After modification by Fe_3O_4, spherical particles of Fe_3O_4 were visible on the surface of h-BN, indicating that the Fe_3O_4 was successfully fabricated on the surface of h-BN.

The XRD pattern of the synthesized products appears in Fig. 2C, which shows that the characteristics peaks at $2\theta = 26.6°$ and 41.6° were assigned to pure phase h-BN, indexed as (002) and (100); the peaks at $2\theta = 30.1°$, 35.5°, 43.1°, 53.5°, 57.0°, 62.7° indexed as (220), (311), (400), (422), (511), and (440) correspond to Fe_3O_4; and diffraction peaks of Fe_3O_4@h-BN related to the components of h-BN and Fe_3O_4 were observed, confirming the formation of Fe_3O_4@h-BN.

The FT-IR spectra of Fe_3O_4, h-BN, and Fe_3O_4@h-BN are shown in Fig. 2D. The absorption band at 580 cm^{-1} matched the Fe–O stretching vibration of Fe_3O_4. The strong peaks at 807 cm^{-1} and 1380 cm^{-1} related to h-BN indicate B–N stretching and B–N–B bending vibrations, respectively. The peaks of both components of h-BN and Fe_3O_4 appeared for Fe_3O_4@h-BN, which further proved the successful synthesis of composites.

Fig. 2E shows the hysteresis loops of Fe_3O_4 and Fe_3O_4@h-BN. The results show that Fe_3O_4 and Fe_3O_4@h-BN exerted a strong magnetic response, and their saturation magnetization values were 77.2 emu g^{-1} and 51.6 emu g^{-1}, respectively. These results illustrate that the magnetization decreases with the increase in the h-BN layer, which indicates the successful combination of

Fe_3O_4 and h-BN. These results prove the excellent magnetic properties of Fe_3O_4@h-BN as an adsorbent for rapid magnetic separation during MSPE.

The elemental composition of the Fe_3O_4@h-BN composite was analysed by XPS (Fig. 2F). The binding energies of B 1s and N 1s were located at 190 eV and 398 eV, respectively, which were ascribed to h-BN. Characteristic peaks revealed for binding energies of 710.58 eV were ascribed to Fe 2p, which suggested the successful formation of a composite consisting of Fe_3O_4 and h-BN. The additional O 1s and C 1s peaks might be caused by the exposure of h-BN to air.

Fig. 2G shows the N_2 adsorption and desorption isotherm obtained by BET testing of Fe_3O_4@h-BN at 77 K. The pore size distribution is shown in Fig. 2H. The shape of the optimum isotherm comes under the type IV isotherm category according to the Union of Pure and Applied Chemistry (IUPAC), and is indicative of multilayer adsorption.[34] The BET surface area was determined to be 23.90 $m^2 g^{-1}$, with a Langmuir surface area of 385.32 $m^2 g^{-1}$, indicating a moderate specific surface area. The BJH pore size distribution (calculated from the desorption branch) showed an average pore diameter of 24.46 nm, confirming the dominance of mesopores (2–50 nm). The differential pore volume curve exhibited a broad peak centered at 20–30 nm, reflecting a polydisperse mesopore distribution. The material possesses a mesoporous framework with moderate surface area and pore volume, and is suitable for adsorption applications.

3.2. Adsorption performance

Adsorption isotherm models were used to describe the distribution of TC, OTC, and CTC molecules on Fe_3O_4@h-BN after an equilibrium state was reached. The adsorption isotherm results and fitting curves of the Langmuir and Freundlich isotherm models of the three TCs are shown in Fig. 3. The adsorption capacity increases with increasing solution concentration, and remained stable when the concentration increased to 400 μg mL^{-1}. The parameters obtained from fitting two isotherm models with the experimental isotherm data are listed in Table 1. The experimental isotherm values fitted well with the Freundlich model, and the correlation coefficients were greater than those obtained with the Langmuir model. This indicated that TC, OTC, and CTC molecules engaged in multilayer adsorption on the surface of Fe_3O_4@h-BN, and the ability of Fe_3O_4@h-BN to adsorb TCs is satisfactory.

The kinetic behavior of TC, OTC, and CTC adsorbed on Fe_3O_4@h-BN was investigated to determine the adsorption capacity with time. The results and fitting curves by pseudo-first order and pseudo-second order kinetic models are shown in Fig. 4. The trend shown by all three TCs can be divided into three zones. In the initial zone, the adsorption rate rapidly increases with time (0–2 min), which can be attributed to the presence of many active surface sites for adsorption. As time proceeds, the adsorption rate gradually slows in the second zone (2–5 min). This indicates increased utilization/occupation of active sites on the surface of Fe_3O_4@h-BN. Finally, the adsorption rate becomes nearly constant with time after 5 min, and equilibrium is achieved in the final zone.
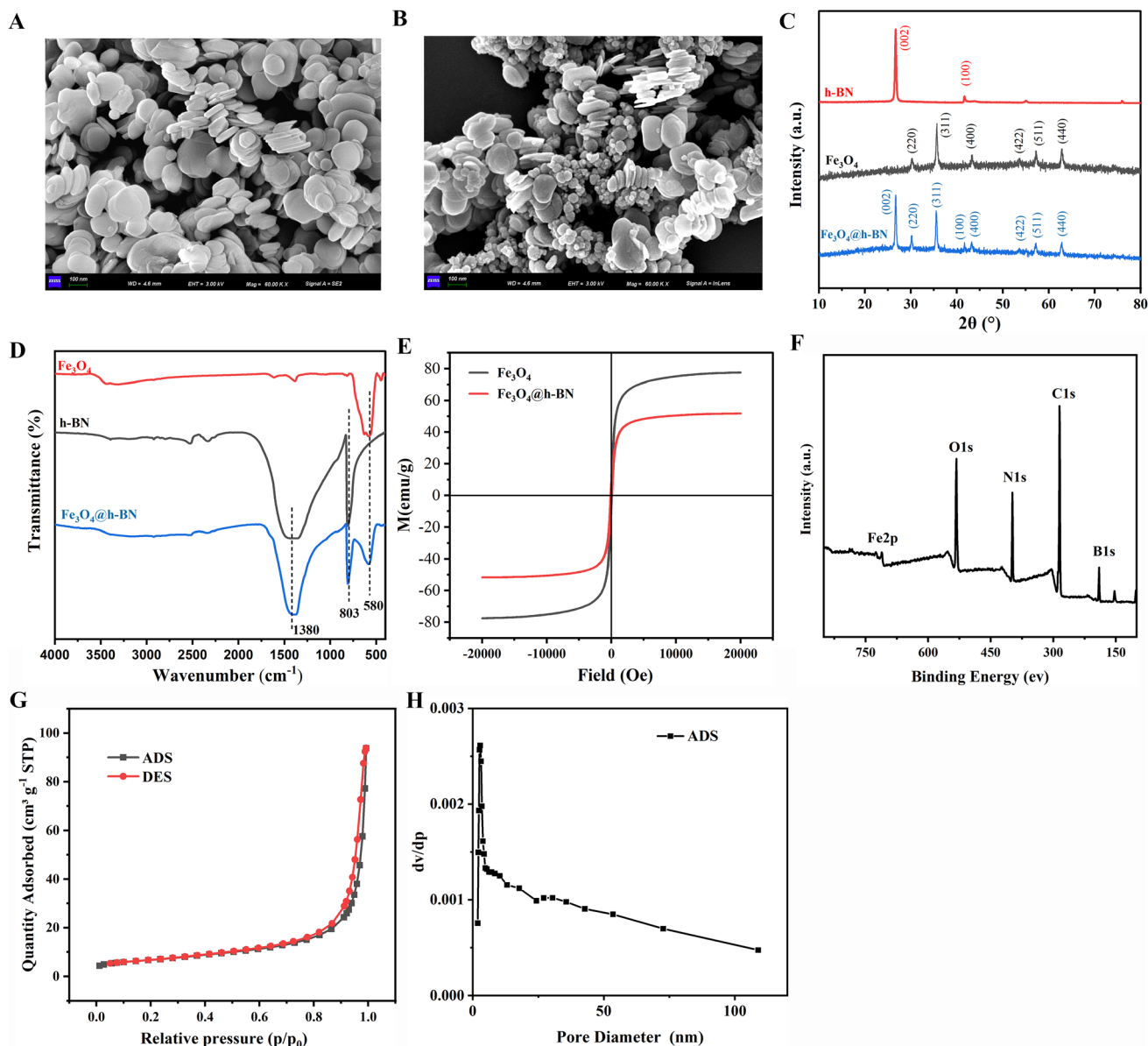
Fig. 2 The characterization of the material: SEM image of (A) h-BN and (B) Fe₃O₄@h-BN; (C) XRD pattern, (D) FT–IR spectrum, (E) VSM analysis, (F) XPS, (G) adsorption and desorption of nitrogen isotherms, and (H) pore distribution of Fe_3O_4@h-BN.

The quantitative results of the two models, including the kinetic constants, equilibrium adsorption capacity, and correlation coefficient (R^2), are shown in Table 2. It was found that the adsorption process fit well with the pseudo-second order kinetic equation, which indicated chemisorption of TCs onto the surfaces of Fe_3O_4@h-BN.[34–36] The adsorption performance of Fe_3O_4@h-BN was attributed to the Fe_3O_4 part and the h-BN part. The large surface area, pore size, and pore volume of h-BN showed π–π interactions between the ring of the h-BN surface and the aromatic rings of TCs, another adsorption mechanism related to chelation between the antibiotics and Fe_3O_4. The combination of these two effects renders Fe_3O_4@h-BN a promising adsorbent for the analysis of tetracycline antibiotics and other pharmaceuticals.

3.3. Optimization of MSPE conditions

3.3.1. Effect of adsorbent dose. The adsorption effect of the adsorbent dose was studied by increasing the amount of Fe_3O_4@h-BN adsorbent from 5 mg to 100 mg. Fig. 5A shows that increasing the absorbent dose from 20 mg to 50 mg led to a higher capacity for adsorption of the three TCs. This can be attributed to the presence of more active sites on the absorbent material. The capacity slowly increased when the amounts of the Fe_3O_4@h-BN adsorbent were more than 50 mg. The constant adsorption capacity at a higher dose can be attributed to the aggregation of the adsorbent, which reduces the number of exposed active sites.

3.3.2. Extraction method. The extraction method can significantly affect the extraction process by influencing the
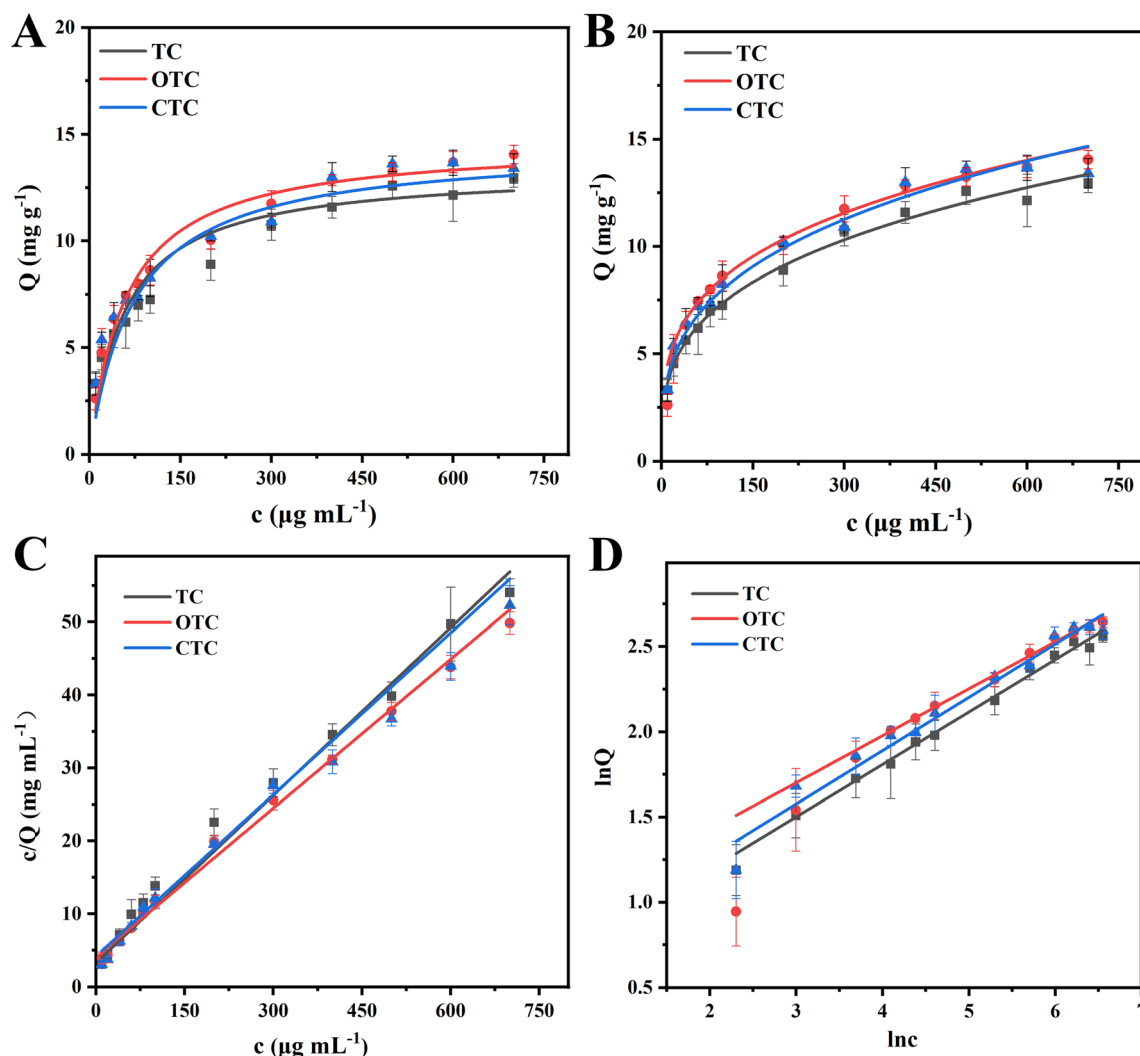
Fig. 3   Adsorption isotherm of TCs by Fe$_3$O$_4$@h-BN and model fitting for the (A) Langmuir and (B) Freundlich models. Fitted curves of (C) Langmuir and (D) Freundlich models of the adsorption.

Table 1   Langmuir and Freundlich adsorption isotherm parameters for TC, OTC, and CTC on Fe$_3$O$_4$@h-BN

TCs	Langmuir			Freundlich		
	Q_m (mg g^{-1})	K_L (mL mg^{-1})	R^2	K_F	n	R^2
TC	13.37	0.0173	0.9401	1.795	3.263	0.9918
OTC	14.65	0.0167	0.9792	2.365	3.594	0.9818
CTC	14.45	0.0135	0.9009	1.893	3.198	0.9811

mass transfer of the target analytes from the adsorbent. In this study, ultrasonication (2 min, 5 min, 10 min), vortexing (1 min, 2 min, 5 min), and oscillation (10 min, 20 min) were adopted for the extraction. Fig. 5B shows that oscillation resulted in greater extraction when compared to the extractions obtained by ultrasonication and vortexing. In addition, the oscillation frequency was also examined, and as shown in Fig. 5C, the efficiency of extracting the three TCs increased when the oscillation frequency was increased from 200 rpm to 500 rpm,

whereas a slight decrease was observed when the oscillation frequency was higher than 500 rpm. The decrease may be due to the desorption of analytes from the adsorbent at high oscillation frequency. Therefore, 500 rpm was chosen as the oscillation frequency for the experimental extraction.

3.3.3.   Effect of pH. Adsorption properties of TCs on Fe$_3$O$_4$@h-BN were investigated by adjusting the pH of the solution from 1.0 to 13.0 with the help of 0.1 mol per L HCl and 0.1 mol per L NaOH. The results are shown in Fig. 5D, the adsorption capacity of Fe$_3$O$_4$@h-BN toward TC, OTC, and CTC gradually increases as the pH value increases, and when the pH value is greater than 6.0, the adsorption capacity rapidly decreases. The highest absorption capacity was observed at pH 5.0 for TC and at pH 6.0 for OTC and CTC, respectively. This indicates that the weak acid environment enables the nanocomposite to adsorb TC, OTC, and CTC more effectively. This is mainly because the pH value of the solution affects the surface charge of the adsorbent and the form of the three TCs in the solution. At low pH, the surface of Fe$_3$O$_4$@h-BN is positively
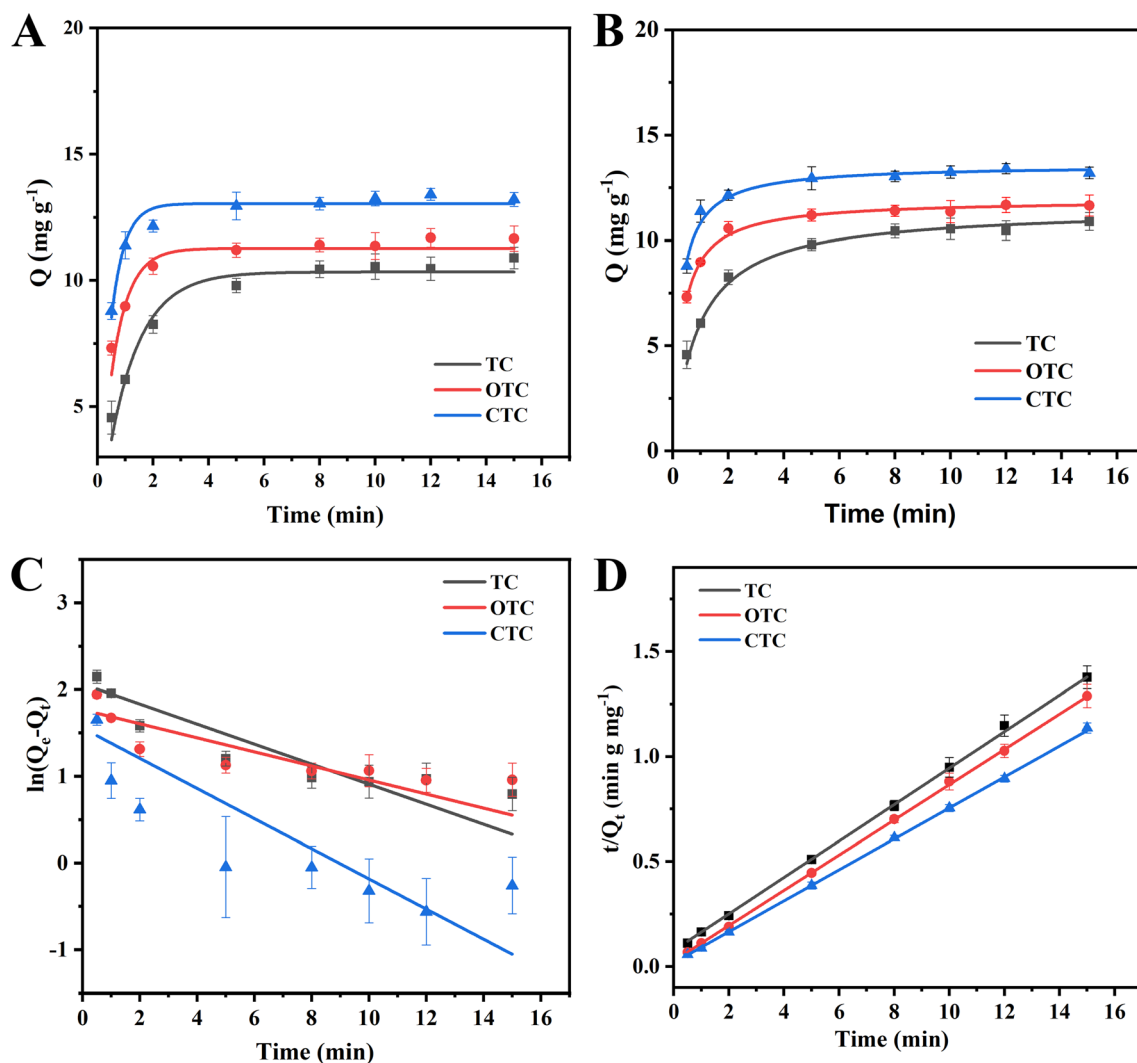
Fig. 4 Adsorption kinetics of TC, OTC, and CTC by Fe_3O_4@h-BN and model fitting for the (A) pseudo-first-order and (B) pseudo-second-order equation. Fitted curves of (C) pseudo-first-order models and (D) pseudo-second-order models of the adsorption.

Table 2 Pseudo-first order and pseudo-second order kinetic parameters for TC, OTC, and CTC on Fe_3O_4@h-BN

TCs	Pseudo-first order constants			Pseudo-second order constants		
	K_1 (min^{-1})	Q_m (mg g^{-1})	R^2	K_2 (g mg^{-1} min^{-1})	Q_m (mg g^{-1})	R^2
TC	0.883	10.34	0.9873	0.0970	11.53	0.9971
OTC	1.620	11.27	0.9340	0.2563	11.93	0.9950
CTC	2.085	13.04	0.9218	0.3601	13.58	0.9848

charged due to the protonation reaction. With increasing pH values, the surface of Fe_3O_4@h-BN becomes negatively charged due to the deprotonation reaction.

In addition, the pH value affects the ionization degree of the TC molecules. TC contains three chemically distinct acidic functional groups: carboxymethyl ($pK_a = 3.3$), phenolic di-ketone ($pK_a = 7.7$), and dimethylamine cation ($pK_a = 9.7$). Thus, when the pH of the solution is less than 3.3, the dominant form in the solution is a cationic species of TC. When the pH is in the range of 3.3–7.7, TC exists without charge. The dominant form

of TC exists as an anionic species when the pH value of the solution is greater than 9.7.[15,29,31] At low pH, Fe_3O_4@h-BN and TC are positively charged, while the highest sorption is observed with a neutral pH, which may be due to the stronger covalent type interactions that are present, as compared to the non-specific electrostatic interactions of Fe_3O_4@h-BN and TC. In addition, TC, OTC, and CTC are susceptible to degradation under acidic conditions and in alkaline solutions, and there-fore, the extraction acidity was set at pH 6.0 for comprehensive consideration.
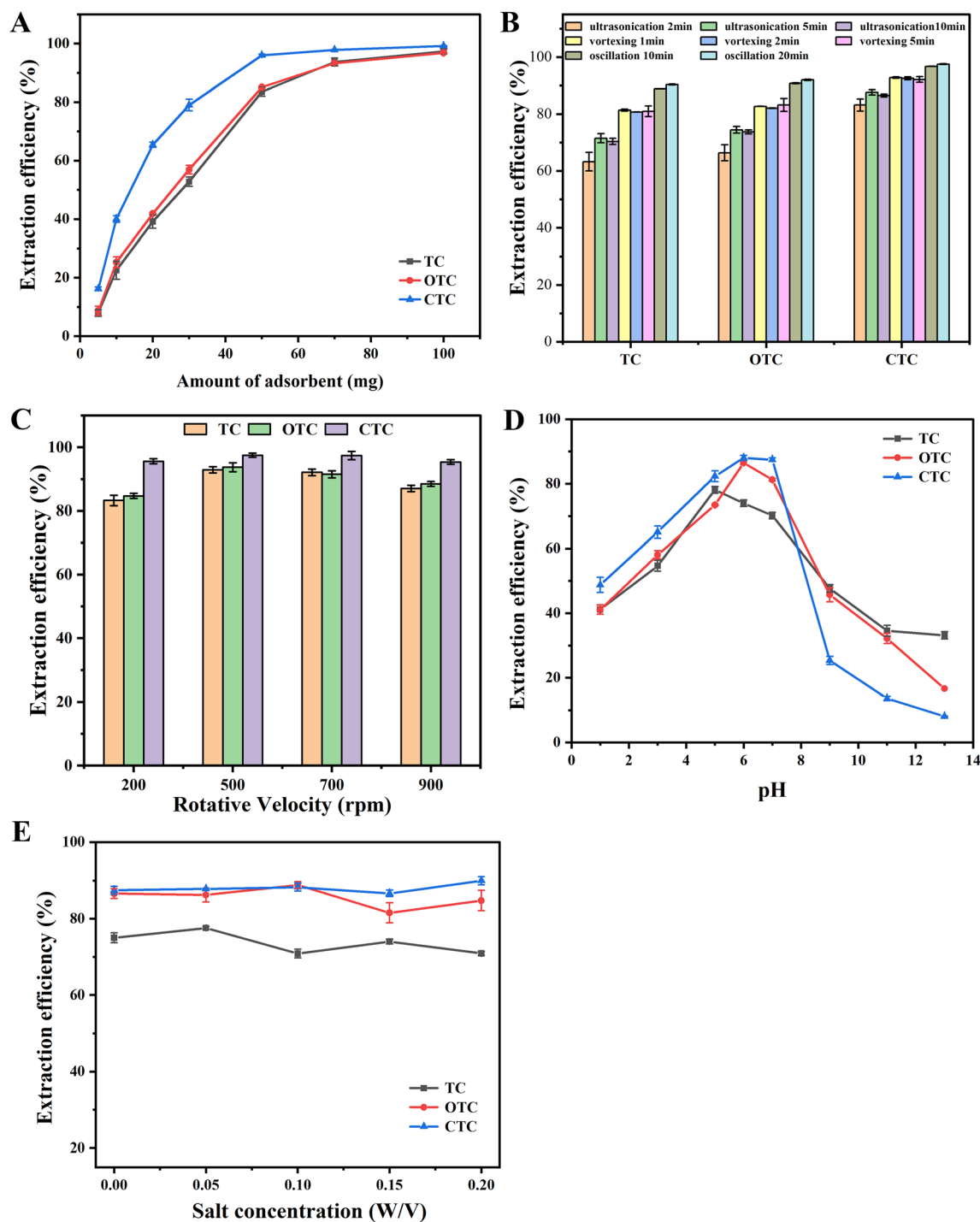
Fig. 5 Extraction effect of (A) amount of adsorbent, (B) extraction method, (C) rotative velocity, (D) pH, and (E) salt concentration on the extraction of TCs.

3.3.4. Effect of ionic strength. The differences in TC adsorption on Fe_3O_4@h-BN as a function of ionic strength were investigated using a series of TC solutions containing different amounts of NaCl (0–20%, m/v). Fig. 5E shows that the adsorption capacity under different ionic strengths exhibited no noticeable change. Although the Na^+ and Cl^- in the solution may interact with molecular TC and Fe_3O_4@h-BN, the

adsorption efficiency is nearly independent of the ionic strength, which indicates that the surface complexation of TC with Fe_3O_4@h-BN is very strong.

3.3.5. Desorption solvent. To select a suitable eluent for the desorption of TCs from Fe_3O_4@h-BN, six solvents were studied separately as eluents: (i) 2.5 mmol per L oxalic acid solution, (ii) methanol–0.1% formic acid, (iii) formic acid–ethyl acetate

containing 20% methanol (1 : 99), (iv) acetonitrile–0.01 mol per L oxalic acid solution (3 : 7), (v) acetonitrile–methanol–0.5% formic acid–water (4 : 1 : 2 : 3) and (vi) acetonitrile–methanol–0.5% formic acid–EDTA buffer–water (4 : 1 : 2 : 0.5 : 2.5). As shown in Fig. 6A, the highest desorption efficiency was achieved for the eluate of acetonitrile–methanol–0.5% formic acid–EDTA buffer–water (4 : 1 : 2 : 0.5 : 2.5) under the same conditions. This may be attributed to the fact that the nucleus of the TCs is a linear tetracyclic structure consisting of four fused rings, which can form chelating complexes by binding to Fe^{3+} cations.

The addition of EDTA buffer can improve the elution of TC by utilizing this multivalent chelating ability of metal cations.

3.3.6. Desorption method. The desorption methods of oscillation (2 min), vortexing (1 min, 2 min), and ultrasonication (5 min) were performed for elution. Fig. 6B shows that the effect of oscillation was superior as compared to that obtained by vortexing or ultrasonication. Therefore, oscillation was chosen for elution in the subsequent experiments. To further investigate the desorption effect, the desorption efficiency and desorption times were studied. The results in Fig. 6C
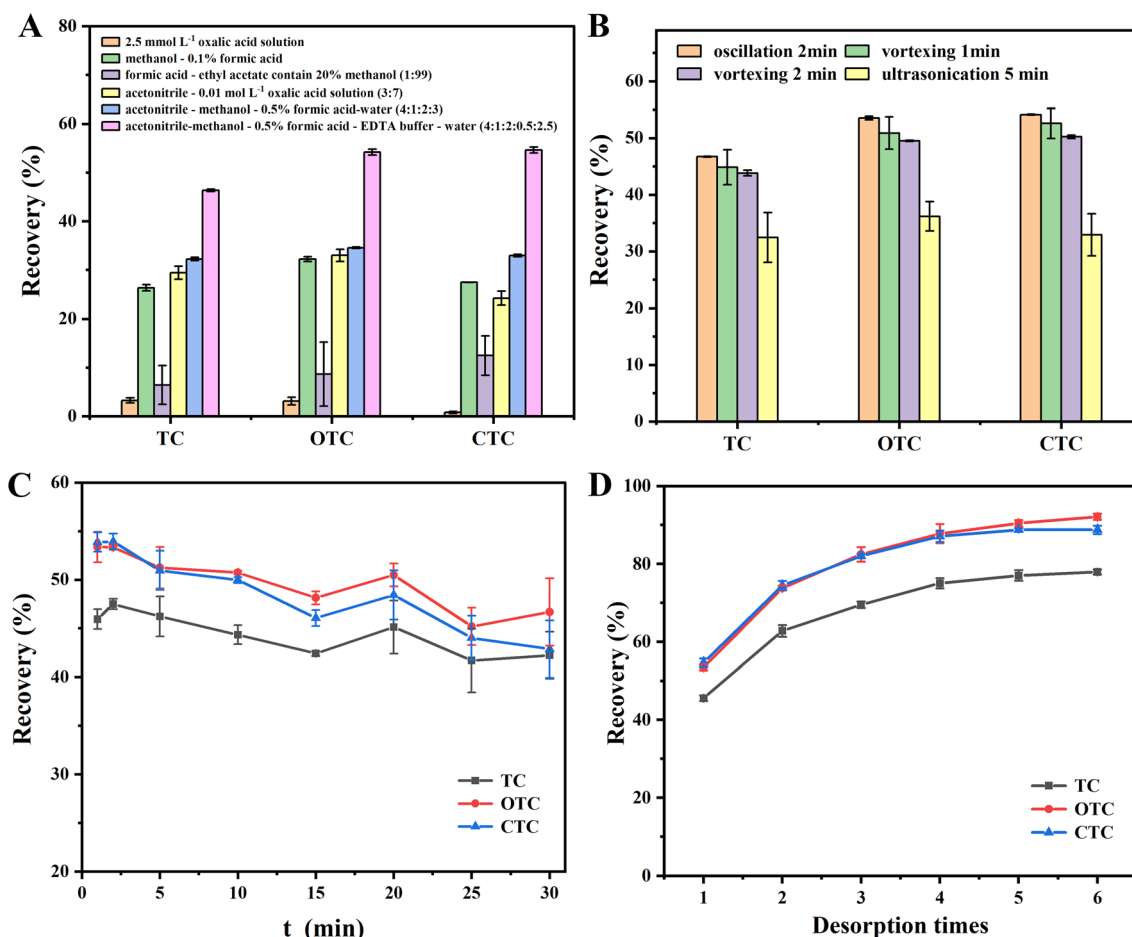

Fig. 6 Desorption effect of (A) elution solvents, (B) desorption method, (C) desorption time, and (D) desorption times.

Table 3 Relevant analysis parameters of the MSPE-HPLC method for determining TC, OTC, and CTC in pork, egg, and milk

Samples	Analytes	Linear range (μg g^{-1})	R^2	LOD (μg g^{-1})	LOQ (μg g^{-1})	Intra-day RSDs (%)	Inter-day RSDs (%)
Pork	TC	0.02–200	0.9930	0.01	0.02	0.6	2.9
	OTC	0.01–200	0.9915	0.005	0.01	0.1	0.9
	CTC	0.06–200	0.9930	0.02	0.06	0.3	2.1
Egg	TC	0.02–200	0.9952	0.005	0.02	0.4	0.4
	OTC	0.02–200	0.9966	0.01	0.02	0.3	2.2
	CTC	0.06–200	0.9940	0.03	0.06	0.6	1.1
Milk	TC	0.01–200	0.9962	0.005	0.01	1.7	6.5
	OTC	0.01–200	0.9917	0.005	0.01	0.8	1.6
	CTC	0.05–200	0.9936	0.01	0.05	1.8	6.3

Table 4 Analysis of TC, OTC, and CTC in pork, eggs, and milk

Samples	Analyte	Spiked (μg g^{-1})	Recovery (%)	RSD (%)
Pork	TC	0	—	—
		0.1	93.2	9.4
		20	87.2	2.8
		100	92.1	0.3
	OTC	0	—	—
		0.1	96.6	7.0
		20	84.2	5.0
		100	92.3	0.9
	CTC	0	—	—
		0.1	87.9	1.7
		20	90.6	1.8
		100	92.3	0.6
Egg	TC	0	—	—
		0.1	100.8	2.2
		20	93.1	1.6
		100	92.8	1.3
	OTC	0	—	—
		0.1	103.8	5.7
		20	103.9	0.8
		100	97.9	1.2
	CTC	0	—	—
		0.1	108.2	9.7
		20	100.9	0.8
		100	95.7	1.5
Milk	TC	0	—	—
		0.1	90.9	1.7
		20	92.8	7.1
		100	94.9	6.0
	OTC	0	—	—
		0.1	94.0	1.3
		20	96.3	6.9
		100	102.6	5.7
	CTC	0	—	—
		0.1	84.1	4.1
		20	99.0	6.5
		100	98.6	6.5

show that when the desorption time was increased from 1 min to 2 min, the desorption efficiency increased, and then decreased after 2 min. Therefore, the optimum resolution time was set at 2 min. The number of desorption times was also

examined in order to elute the maximum amount of the compounds from the adsorbent. The results in Fig. 6D show that after 4 repetitions of desorption, the recoveries of TC, OTC, and CTC were 75.00%, 87.80%, and 87.08%. Further increase in the number of desorption times resulted in only a slight increase in desorption efficiency, and therefore, 4 repetitions of elution were chosen as the number of desorption times.

3.4. Method evaluation

To verify that the Fe$_3$O$_4$@h-BN-based MSPE-HPLC method can be used to successfully extract TC, OTC, and CTC from pork, egg, and milk samples, the proposed method was validated by the parameters of limit of detection (LOD), limit of quantification (LOQ), linear range, determination coefficients (R^2), and intra-day and inter-day relative standard deviations (RSDs), which are summarized in Table 3. A standard curve was established using pork, egg, and milk samples containing varying concentrations because the influence of the matrix could not be entirely excluded.

The results indicated that three TCs in the pork, egg, and milk samples exhibited a good linear relationship in the range of 0.01–200 μg g^{-1}. LODs and LOQs were determined as spiked concentrations with signal-to-noise ratios of 3 (S/N = 3) and 10 (S/N = 10), respectively. The LODs of the proposed method for the three TCs ranged from 0.005–0.03 μg g^{-1}, and their LOQs ranged from 0.01–0.06 μg g^{-1}. For each test, three parallel analyses were performed to derive reliable results. Additionally, the intra-day RSDs of pork, egg, and milk are 0.1–1.8%, and the inter-day RSDs are 0.4–6.5%. These results illustrate that low limits and satisfactory accuracy were obtained with the established method, and therefore, it is suitable for practical application.

3.5. Sample analysis

For method recovery studies, three different concentrations of TC, OTC, and CTC were added to blank pork, egg, and milk samples with concentrations of 0.1, 20, and 100 μg g^{-1}. As shown in Table 4, the measured recoveries of the three TCs for pork, egg, and milk were 84.2–96.6%, 92.8–108.2%, and 84.1–102.6%, respectively, and the RSDs for pork, egg, and milk were 0.3–9.4%,
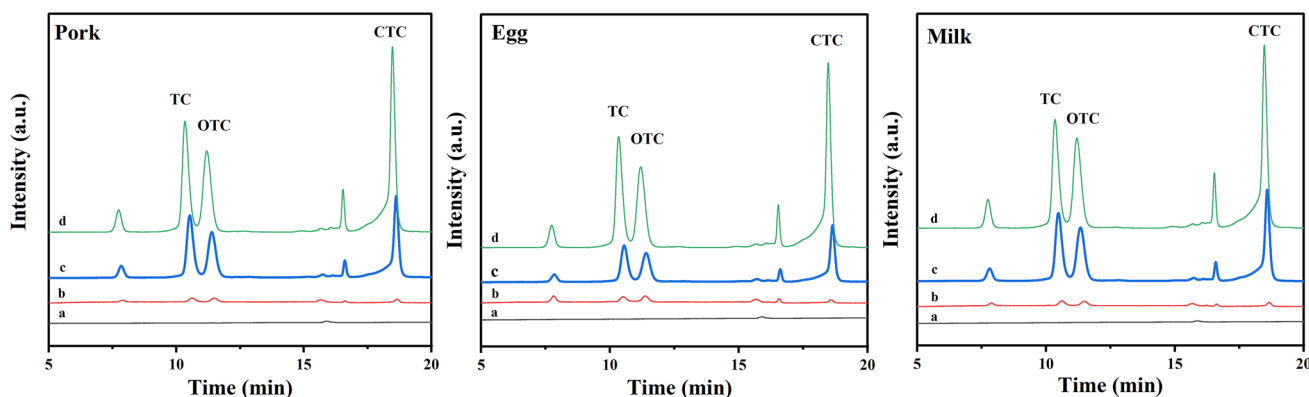

Fig. 7 The chromatograms of (a) blank sample and spiked pork, egg, and milk samples with concentrations at (b) 0.1 μg g^{-1}, (c) 20 μg g^{-1}, and (d) 100 μg g^{-1}.

0.8–9.7%, and 1.3–7.1%, respectively. High recoveries and low RSDs were obtained using this method, which suggests good applicability of the Fe_3O_4@h-BN-based MSPE-HPLC method for the analysis of TCs in pork, egg, and milk. Typical chromatograms of pork, egg, and milk samples are shown in Fig. 7.

3.6. Repeatability

The repeatability test was performed using spiked milk samples. As shown in Fig. S1, the results indicate that there was no significant change in the extraction efficiency of the nanoparticles after 5 repeated uses. The good repeatability of Fe_3O_4@h-BN was proved.

3.7. Comparison with other reported methods

To evaluate the Fe_3O_4@h-BN-based method, the linear range, LODs, recovery, and RSDs were compared with others reported in the literature. As shown in Table S1, the established method showed similar recovery, accuracy, and lower LODs, which proves that comparable sensitivity was obtained with the Fe_3O_4@h-BN-based method developed in this work. In addition, the approach is user-friendly, time-saving, and easy to operate with the assistance of an applied magnetic field.

4. Conclusions

The highly efficient adsorbent Fe_3O_4@h-BN with a high surface area was synthesized by a simple one-step coprecipitation method and characterized in this study. Fe_3O_4@h-BN was able to significantly adsorb TC antibiotics due to $\pi-\pi$ interaction and the chelation interaction of Fe_3O_4@h-BN. Using MSPE-HPLC, the synthesized nanocomposites were tested for TC, OTC, and CTC in pork, egg, and milk samples. Under optimized experimental conditions, the measured recoveries and RSDs for pork, egg, and milk were 84.1–108.2% and 0.3–9.7%, respectively. With the one-step reaction, multiple modification steps at high temperature are unnecessary, and this simplifies the synthesis process, and saves time and energy. The results demonstrate the considerable potential of Fe_3O_4@h-BN as an adsorbent for the detection of antibiotics in food samples.

Author contributions

Junmei Li: writing – original draft, project administration, methodology. Weiran Wang: visualization, investigation, formal analysis. Yupeng Sun: visualization, validation. Yan Fu: visualization, validation. Haoqi Zhang: visualization, validation. Bingrong Wang: visualization, validation. Chunying Wang: supervision, conceptualization. Xue Xiong: writing – review and editing, supervision, project administration, funding acquisition, conceptualization.

Conflicts of interest

The authors declare that they have no known competing financial interests or personal relationships that could have appeared to influence the work reported in this paper.

Data availability

The data that support the findings of this study are available from the corresponding author upon reasonable request.

Supplementary information file contains Fig. S1 and Table S1 is available. See DOI: **https://doi.org/10.1039/d5ay01104c**.

Acknowledgements

References

1 D. Chang, Y. Mao, W. Qiu, Y. Wu and B. Cai, *Toxics*, 2023, **11**, 214.

2 X. Zhang, T. Cai, S. Zhang, J. Hou, L. Cheng, W. Chen and Q. Zhang, *J. Hazard. Mater.*, 2024, **463**, 132862.

3 J. Leichtweis, Y. Vieira, N. Welter, S. Silvestri, G. L. Dotto and E. Carissimi, *Process Saf. Environ. Prot.*, 2022, **160**, 25–40.

4 X. Wang, Y. Dong, Y. Luan, S. Tian, C. Li, Y. Li and J. Zhou, *J. Hazard. Mater.*, 2024, **473**, 134681.

5 A. Khezerlou, M. Tavassoli, R. Abedi-Firoozjah, M. Alizadeh Sani, A. Ehsani and R. S. Varma, *Sci. Rep.*, 2025, **15**, 502.

6 A. Khezerlou, M. Tavassoli, M. Alizadeh Sani, Z. Ghasempour, A. Ehsani and B. Khalilzadeh, *Food Chem.*, 2023, **20**, 100883.

7 Y. Yang, S. Yin, L. Wu, Y. Li and C. Sun, *J. AOAC Int.*, 2021, **104**, 1549–1558.

8 K. F. Kayani, *Sep. Purif. Technol.*, 2025, **364**, 132418.

9 Y. Amangelsin, Y. Semenova, M. Dadar, M. Aljofan and G. Bjørklund, *Antibiotics*, 2023, **12**, 440.

10 C. Li, Z. Tian, L. Bao, Y. Shi, Y. Ji, M. Cui, J. Xing and Z. Zhao, *Food Chem.*, 2024, **446**, 138854.

11 J. Zhang, Y. Yi, S. Chengjun and L. Wu, *Int. J. Environ. Anal. Chem.*, 2024, **104**, 8102–8131.

12 A. K. El-Deen and C. M. Hussain, *Trends Environ. Anal. Chem.*, 2023, **39**, e00209.

13 A. Karataş, T. Oymak and A. Çelik, *J. Pharm. Biomed. Anal.*, 2024, **249**, 116336.

14 X. H. Zhao, A. Y. Wang, L. Z. Zhai, J. H. Gao, S. Z. Lyu, Y. S. Jiang, T. Zhong, Y. Xiao and X. Yu, *Anal. Chim. Acta*, 2024, **1285**, 342020.

15 F. Poormand, S. Farhadi, A. Zabardasti and F. Mahmoudi, *Inorg. Chem. Commun.*, 2024, **161**, 111978.

16 Y. Yang, S. Yin, D. Yang, Y. Jiang, Y. Li, C. Zhou and C. Sun, *Anal. Bioanal. Chem.*, 2019, **411**, 507–515.

17 C.-Y. Xu, Y.-Y. Cui and C.-X. Yang, *TrAC, Trends Anal. Chem.*, 2025, **185**, 118171.

18 M. Aouled Abdallah, R. Ben Sghaier, M. Zougagh, L. Latrous and A. Megriche, *Anal. Methods*, 2024, **16**, 1870–1879.

19 J. Chen, X. He and Y. Wang, *Anal. Methods*, 2025, **17**, 3132–3144.

20 S. Yu, X. Wang, H. Pang, R. Zhang, W. Song, D. Fu, T. Hayat and X. Wang, *Chem. Eng. J.*, 2018, **333**, 343–360.

21 G. Dee, O. O'Donoghue, E. Devitt, T. Giroud, A. Rafferty, L. Gannon, C. McGuinness and Y. K. Gun'ko, *ACS Omega*, 2024, **9**, 4347–4358.

22 D. Liu, W. Lei, S. Qin, K. D. Klika and Y. Chen, *Phys. Chem. Chem. Phys.*, 2016, **18**, 84–88.

23 D. Li, Z. W. Liu, Q. N. Meng, G. X. Xing, K. Zhao and Y. F. Tang, *Environ. Res.*, 2025, **269**, 120871.

24 C. Bläker, T. Jähnichen, J. Hojak, L. Gehrke, C. Pasel, T. Paschke, F. Dreisbach, D. Enke and D. Bathen, *ACS Omega*, 2024, **9**, 42721–42733.

25 T. Zheng, H. Wu, Z. Han, L. Chen, B. Tang, P. Cui, H. Liu, Y. Chao, W. Zhu and Z. Liu, *Sep. Purif. Technol.*, 2024, **340**, 126648.

26 B. Wang, W. Bai, G. Wang, K. Guo, H. Duan, Y. Xue and C. Tang, *Colloids Surf., A*, 2022, **632**, 127749.

27 W. J. Bai, B. Z. Wang, S. B. Yang, S. Yan, C. C. Cao, Z. Zhou, J. W. Ji, K. Guo and C. C. Tang, *ChemPlusChem*, 2022, **87**, e202200290.

28 Q. Song, J. Liang, Y. Fang, Z. Guo, Z. Du, L. Zhang, Z. Liu, Y. Huang, J. Lin and C. Tang, *Chem. Eng. J.*, 2020, **394**, 124985.

29 U. Lawal Usman, B. Kumar Allam, N. Bahadur Singh and S. Banerjee, *J. Mol. Liq.*, 2022, **354**, 118833.

30 M.-J. Li, N. Li, G. Xu, L.-X. Zhao, X. Chen, Y. Zhao and R.-S. Zhao, *Food Chem.*, 2021, **348**, 129103.

31 C. Zhang, Y. He, F. Li, H. Di, L. Zhang and Y. Zhan, *J. Alloys Compd.*, 2016, **685**, 743–751.

32 Z.-Q. Duan, Y.-T. Liu, X.-M. Xie, X.-Y. Ye and X.-D. Zhu, *Chem.–Asian J.*, 2016, **11**, 828–833.

33 M. J. Carrera Espinoza, K.-S. Lin, M.-T. Weng, S. C. Kunene, Y.-S. Lin and S.-Y. Liu, *Colloids Surf., B*, 2023, **222**, 113129.

34 R. S. Bangari and N. Sinha, *J. Mol. Liq.*, 2019, **293**, 111376.

35 M. Musah, Y. Azeh, J. Mathew, M. Umar, Z. Abdulhamid and A. Muhammad, *Caliphate Journal of Science and Technology*, 2022, **4**, 20–26.

36 T. Liu, C. Sang, Y. Liu, B. Shao and G. He, *Food Chem.*, 2025, **492**, 145624.